EGTRIB Journal
JOURNAL OF
THE EGYPTIAN SOCIETY OF TRIBOLOGY
VOLUME 22, No. 1, January 2025, pp. 55 - 80 **ISSN 2090 - 5882**
(Received October 18. 2024, Accepted in final form November 05. 2024) **jest.journals.ekb.eg**

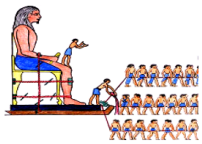

OPTIMIZATION OF THE ELECTROWINNING PROCESS FOR PRODUCTION OF ELECTROLYTIC MANGANESE POWDER FROM PASTE OF $ZnMnO_2$ SPENT PRIMARY BATTERIES

Enas Atef Mohamed Said[1], Ashour Owais[2], Sherine Araby Mansour Ali[1], Essam Ahmed[2] and Ramadan Ibrahim ElSoeudy[1]

[1]Mechanical Engineering Department, Faculty of Engineering, Suez Canal University, Ismailia, Egypt,
[2]Department of Metallurgical and Materials Engineering, Faculty of Petroleum and Mining Engineering, Suez University, 43221 Suez, Egypt.

ABSTRACT
This study involved the statistical analysis and optimization of the electrowinning process for producing electrolytic manganese powder from the paste of used $ZnMnO_2$ primary batteries, utilizing response surface methodology (RSM). The analysis considered the effect of electrolyte temperature (30 - 50 ℃), stirring rate (250 - 350 rpm), distance between the anode and the cathode (3 - 10 cm), and current density (200- 600 A/m^2) on the cathodic current efficiency, specific energy demand, and powder productivity. The experimental design utilized a Box-Behnken approach, employing quadratic polynomial equations to predict the mathematical models. The findings suggest that the proposed models effectively predict responses within the parameters of the electrowinning process utilized. The most important factors influencing cathodic current efficiency, specific energy demand, and productivity are the current density, the second-order effects of both current density and stirring rate, the distance between the anode and cathode, and the interactions between temperature and current density. Additionally, it was determined that RSM serves as an effective tool for optimizing the electrowinning process.

KEYWORDS
Spent Zn-MnO_2, manganese, design of experiment, response surface methodology, optimization.

INTRODUCTION
The Zn-MnO_2 primary batteries are a widely recognized and established technology used across various applications, such as electronic toys, small devices, and portable gadgets, [1, 2]. The usage of these batteries surpasses that of other types due to their easy manufacturing process and safety for transport. As they are non-rechargeable (primary cells), they become unusable once depleted and need to be discarded, [3]. Figure 1 illustrates a cross-section of typical cylindrical primary Zn-MnO2 batteries. These batteries consist of manganese dioxide (MnO_2) used as the positive electrode, metal zinc (Zn) as the negative electrode, an aqueous solution of potassium hydroxide (KOH for alkaline Zn-MnO_2 batteries) or ammonium chloride (NH_4Cl for neutral Zn-MnO_2 batteries) as the electrolyte, and a small amount of conductive and corrosion inhibiting additives, [4].

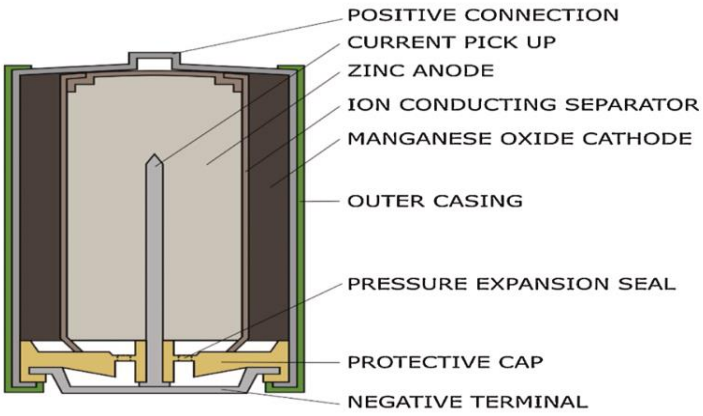

Fig. 1 Cross-sectional schematic diagram of a cylindrical spent primary Zn-MnO_2 batteries, [5].

Zinc and manganese can be extracted from batteries using various recovery methods, primarily pyrometallurgical and hydrometallurgical processes. Extensive comparisons of these techniques have been conducted in past studies, [6, 7]. The pyrometallurgical method consumes significant energy due to its high-temperature requirements, [6] and can produce harmful gas emissions, such as carbon dioxide, carbon monoxide, and sulfur dioxide, as well as dust and volatile organic compounds, [8]. Consequently, this method often necessitates strict emissions controls, [3]. On the other hand, the hydrometallurgical process recovers metals from ores and waste materials using aqueous solutions with various chemicals. This involves dissolving the anodes and cathodes in acidic or alkaline solutions, followed by metal recovery through precipitation, extraction, or electrolysis. This approach is considered superior for recycling batteries since it minimizes gas emissions and requires less energy. Examples include the electrowinning of lead from chloride leach liquor, [9], packed bed electrolysis for copper powder production, [10], and other studies examining the effects of material shape and electrolyte characteristics on copper and manganese recovery, [11 - 17].

Electrolytic manganese powder plays an essential role in the cathodes of Zn MnO_2 alkaline batteries. The increased need for manganese is tied to steel production. Manganese and its derivatives are employed across multiple industries for applications such as steelmaking, manufacturing dietary supplements, producing fertilizers, making batteries, and developing specialty chemicals, [18, 19]. Additionally, they serve as drying agents, catalysts for dyes and varnishes, and color removers in the glass sector, [20].

Recently, the design of experiments (DoE) has become a widely used approach to establish numerical relationships between various input parameters impacting the electrolytic process variables to pinpoint the parameters that lead to the desired electrolytic product. This statistical method is an effective way to plan experiments, enabling the analysis of data for valid and objective conclusions. The two primary applications of experimental design are screening, which identifies the factors that affect the experiment, and optimization, which determines the best settings or conditions for the experiment.

The traditional optimization approach involves adjusting one process condition while keeping others constant. However, when dealing with multiple process variables, analyzing the entire system becomes increasingly challenging using this method. Recent statistical designs address this issue by considering all process parameters at the same time, allowing for a comprehensive evaluation of their collective effects. Response surface methodology (RSM) is recognized as one of the most prevalent optimization techniques used to analyze the performance of industrial processes, [21 - 24]. RSM has been effectively utilized in various studies focused on process analysis, optimization, and variable formulation, [25].

According to the authors' knowledge, there is currently no information in the public domain regarding the characterization and optimization of the electrowinning process for generating electrolytic manganese powder from the paste of used $ZnMnO_2$ primary batteries using a statistical method. Therefore, this research intends to create mathematical models utilizing Response Surface Methodology (RSM) to predict, characterize, and assess the cathodic current efficiency, specific energy requirement, and powder productivity in the electrowinning process for the production of electrolytic manganese powder from the paste of used $ZnMnO_2$ primary batteries. Additionally, the optimization of the electrowinning process will be addressed.

EXPERIMENTAL WORKS

Material

Spent $ZnMnO_2$ batteries were broken and separated from the external papers and paste of batteries collected, which was then crushed into a powder to ensure a uniform consistency. This roasted battery powder was leached using ascorbic acid ($C_6H_8O_6$) as a reducing agent in a sulfuric acid (H_2SO_4) solution. Following the leaching step, cementation for selective removal of zinc ions was performed using manganese powder (Mn). More details on the used material and experiments were found in the purification of Manganese electrolyte solution from the leaching of Zn-MnO_2 spent batteries using the cementation technique, [26]. After purification of the Mn electrolyte solution from zinc, the solution contains 34.75 gm/L of Manganese ions.

The used electrolytic cell for the extraction of Manganese from the paste of used $ZnMnO_2$ primary batteries is shown in Fig. 2 and it consists of the following:

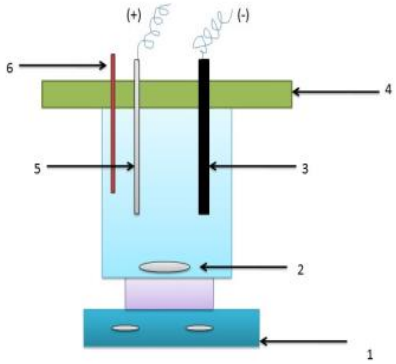

1. **Hot plate with a magnetic stirrer.**
2. **Rotating fish.**
3. **Stainless steel sheet cathode (-).**
4. **Stand & cell plastic cover.**
5. **Anode of graphite.**
6. **Thermometer.**

Fig. 2 Components of electrolytic cell, [17].

A hot plate with a magnetic stirrer (DAIHAN SCIENTIFIC CO, Korea) was used for heating up and stirring the electrolyte, and the direct current was supplied to the electrodes by a power supply (GW Instek, DC Power supply SPS -1820, Taiwan). Extra details on the obtained results of the electrowinning process of production of manganese from the paste of used $ZnMnO_2$ primary batteries were found in (Said et al, under publication).

DESIGN OF EXPERIMENTS AND STATISTICAL APPROACH

RSM is a widely used statistical modeling technique that helps identify key processing parameters, quantify their relationships with specific measured outputs, and determine the optimal responses of interest, [28 - 30]. In the RSM, various methods and tools for constructing regression models and assessing their adequacy are utilized. Let y represent the observed value of a response variable influenced by the levels of k quantitative factors, denoted as x_1, x_2, ..., x_k. For the statistical analysis, the three independent variables were designated as X_1, X_2, and X_3, respectively, and were coded according to Eq. (1) as follows, [31]:

$$Xi = \frac{Xi - Xo}{\Delta Xi} \quad (1)$$

Where X_i and x_i are the coded and real values of an independent variable, respectively, while, Xo is the real value of an independent variable at the central point and ΔXi is the step change value, [31]:

The response function is then written as:

$$Y = f(x_1, x_2, \ldots\ldots x_k)\varepsilon \quad (2)$$

Where ε is the noise or error term in observing the response.

Contour plotting is frequently used to depict the predicted response surface graphically. The quadratic response model consists of all the linear terms, square terms, and linear interactions and can be written as the subsequent equation [31]:

$$Y = b0 + \sum_{i=1}^{n} bi_{xi} + \sum_{i=1}^{n} b_{ii} x_{2ii} + \sum_{i=1}^{n} \sum_{j=1}^{n} b_{ij} x_i x_j + \varepsilon \quad (3)$$

The method the of electrowinning process involves multiple variable parameters that impact the optimal values of the parameters and the responses of interest. To optimize and evaluate the primary effects of the electrowinning process, a four-factor, three-level box-Behnken statistical design with full replication was employed in this study. The temperature of the electrolyte, current density, rate of electrolyte stirring, and the distance between the anode and cathode are the factors that can be controlled in the electrolytic refining process. On the other hand, the efficiency of the cathodic current, energy consumption, and the amount of powder produced are outputs that depend on these variables. Experiments were conducted by changing one process parameter while keeping the rest constant to determine the constraints of the process input parameters. Tables 1 - 3 provide summary of the different independent process variables, experimentally measured responses, and design matrix in the study. A series of 25 electrolysis experiments were conducted using electrowinning techniques, with various process parameters based on the design matrix.

Table 1 Independent process variables and experimental design levels.

Variable		Unit	Goal	Code		
				Low	Medium	High
				-1	0	+1
Electrolyte Temperature	A	℃	Minimize	30	40	50
Stirring Rate	B	Rpm	Minimize	0	100	200
Distance between anode and cathode	C	Cm	Minimize	3	6.5	10
Current Density	D	A/m^2	Minimize	200	400	600

Table 2 Goals of experimentally measured responses.

Response		Unit	Goal
Cathodic Current Efficiency	CE	%	Maximize
Specific Energy Demand	SE	KWh/Kg	Minimize
Powder Productivity	PP	g/Ah	Maximize

Table 3 Design matrix with code independent process variables.

Run	Factor 1	Factor 2	Factor 3	Factor 4
	A: Electrolyte Temperature	B: Stirring Rate	C: Distance between anode and cathode	D: Current density
1	40	200	3	400
2	30	100	6.5	600
3	40	0	3	400
4	50	100	6.5	600
5	50	200	6.5	400
6	30	100	10	400
7	40	0	6.5	200
8	40	100	10	200
9	40	100	6.5	400
10	50	100	6.5	200
11	40	0	6.5	600
12	30	0	6.5	400
13	30	100	3	400
14	40	200	6.5	200
15	40	200	10	400
16	40	0	10	400
17	40	200	6.5	600
18	50	100	10	400
19	30	100	6.5	200
20	30	200	6.5	400
21	40	100	3	200
22	40	100	3	600
23	50	0	6.5	400
24	40	100	10	400
25	50	100	3	400

Evaluation of Variance and Creation of Models

The significant parameters and the best level for each parameter that was evaluated against regression can be found using analysis of variance (ANOVA). The F test was used on individual terms of the model to determine the significance of the regression model and identify the significant terms and their respective levels of significance. The model terms are considered significant if the value of "prob > F" is less than 0.05.

Additionally, the step-wise regression technique was used to remove any insignificant model terms automatically. The "lack of fit value" indicates how much the actual data varies around the fitted model. If the F test results show that the lack of fit is not significant, it implies that the model accurately represents the data, which is an ideal outcome. R^2 and the adjusted R^2 values are two additional criteria used in this modeling process. R^2 is used to indicate the adequacy of a fitted regression model. R^2 is a measure of the variation around the mean, and the adjusted R^2 value is a measure of the variation around the mean of the adjusted model terms. Scatter plots were also utilized for regression analysis. Perturbation curves and response surface plots were calculated for every model."Adeq Precision" measures the signal-to-noise ratio of each model. If the ratio is > 4, it indicates that the model is desirable, [31]. Based on the fit summaries, the suitable response models for the response factors should be selected. The experimental results of the cathodic current efficiency, specific energy, and productivity are listed in Table 4. The measured responses were analyzed by the design expert software Design-Expert V.13.

Table 4 Experimentally measured responses.

Run	Response 1	Response 2	Response 3
	Cathodic Current Efficiency %	Energy Demand (KWh/Kg)	Productivity (g/A.h)
1	83.6	10.5	0.725
2	85.9	13.5	0.725
3	75.7	9.7	0.689
4	84.9	13.5	0.812
5	88.4	12.5	0.825
6	79.2	12.07	0.812
7	74.9	7.5	0.725
8	82.93	7.76	0.85
9	84.56	10.68	0.867
10	87.7	10.5	0.825
11	82.5	12.6	0.799
12	80.6	13	0.752
13	83.6	10.7	0.799
14	82.7	7.76	0.725
15	82.85	9.82	0.85
16	79.2	11.7	0.812
17	86.1	12.072	0.83
18	85.85	8.7	0.875
19	75.4	7.76	0.725
20	81.7	12.2	0.785
21	68.5	7.76	0.625
22	83.9	12.5	0.725
23	87.2	10.35	0.825
24	91.38	10.681	0.937
25	78.9	12.5	0.725

Cathodic Current Efficiency Model

The cathodic current efficiency is viewed as a crucial factor for evaluating the effectiveness of the electrolysis process. Additionally, it is a crucial factor in terms of energy consumption and the rate at which powder is deposited. It can be defined as

the ratio of the actual deposited amount of material at the electrode to the deposited amount which is calculated using Faraday's law, by the passage of the same charge, assuming that no side reactions take place at the electrode. It depends on many factors such as the temperature, the current density, the stirring rate, the presence of additives and /or impurities in the electrolyte, the compositions and properties of the electrolyte, and the nature of the electrodes and the electrodeposit, [32].

This research only focused on analyzing how temperature, current density, stirring rate, and the distance between the anode and cathode impact the cathodic current efficiency. Table 5 provides the results of the analysis of variance (ANOVA) for the cathodic current efficiency and Table 6 shows fit statistics for the cathodic current efficiency quadratic model.

Table 5 ANOVA for cathodic current efficiency quadratic model.

Source	Sum of Squares	Df	Mean Square	F-value	p-value	
Model	492.99	14	35.21	3.34	0.0305	**Significant**
A-temperature	56.29	1	56.29	5.35	0.0433	**Significant**
B-stirring rate	53.13	1	53.13	5.05	0.0485	**Significant**
C-distance	30.85	1	30.85	2.93	0.1177	
D-current density	60.75	1	60.75	5.77	0.0372	**Significant**
AB	0.0025	1	0.0025	0.0002	0.9880	
AC	29.11	1	29.11	2.76	0.1273	
AD	44.22	1	44.22	4.20	0.0676	
BC	4.52	1	4.52	0.4289	0.5273	
BD	4.41	1	4.41	0.4189	0.5321	
CD	63.76	1	63.76	6.06	0.0336	**Significant**
A^2	2.47	1	2.47	0.2345	0.6386	
B^2	21.15	1	21.15	2.01	0.1868	
C^2	59.71	1	59.71	5.67	0.0385	**Significant**
D^2	47.96	1	47.96	4.56	0.0586	
Residual	124.96	10	10.33			
Cor Total	598.27	24				

Table 6 Fit statistics for cathodic current efficiency quadratic model.

R^2	Adjusted R^2	Predicted R^2	Adeq Precision
0.8240	0.577	- 0.3595	7.4840

The F-value of 3.34 from the ANOVA results implies the model is significant. Values of "Prob > F" < 0.05 indicate model terms are significant. There is only a 3.05 % chance that an F-value this large could occur due to noise. The analysis of variance indicates that for the cathodic current efficiency model, the main effect of the current density (A), (B), (D), (CD,) and (C^2) are significant model terms. The model terms are not significant if the obtained value areas are greater than 0.1.

The predicted R^2 of 0.8240 was close to the adjusted R^2 of 0.5777. "Adeq Precision'' measures the signal-to-noise ratio. A ratio > 4 is desirable. In this mode, the ratio of 7.4840 indicates an adequate signal. This model can be used to negative the design space. A negative predicted R^2 implies that the overall mean may be a better predictor

of your response than the current model in some cases, a higher-order model may also predict better. The ultimate mathematical equation representing the cathodic current efficiency based on coded factors, as determined by design expert software, is presented below.

$$\text{Cathodic current efficiency} = 87.83 + 2.17*A + 2.10*B + 1.67*C + 2.46*D + 0.0250*AB + 2.70*AC - 3.32*AD - 1.06*BC - 1.05*BD - 5.01CD - 0.8655*A^2 - 2.53*B^2 - 4.65*C^2 - 4.00*D^2 \quad (4)$$

Specific Energy Demand Model

The ANOVA outcomes for the simplified quadratic model of the specific energy demand calculations can be found in Table 7. The model F-value of 7.86 indicates that the model is significant. There is only a 0.12% chance that an F-value this large could occur due to noise. The values of "Prob > F" < 0.05, imply that the model terms are significant. In this case (D), and (AC) are significant model terms. Values greater than 0.1000 indicate the model terms are not significant. A high F-value for a parameter indicates that the impact of that parameter on the refining process characteristics is significant. The results show that the highest value is F at a current density of about 65.49. Table 8 shows the fit statistics for the specific energy demand quadratic model. The predicted R^2 of 0.4751 is not as close to the adjusted R^2 of 0.8001 as one might normally expect. ‘‘Adeq Precision” measures the signal-to-noise ratio. A ratio greater than 4 is desirable. The ratio of 9.997 indicates an adequate signal. This model can be used to negative the design space.

Table 7 ANOVA for specific energy demand quadratic model.

Source	Sum of Squares	Df	Mean Square	F-value	p-value	
Model	84.41	14	6.03	7.86	0.0012	**Significant**
A-temperature	0.1160	1	0.1160	0.1513	0.7054	
B-rpm	3.333E-07	1	3.333E-07	4.347E-07	0.9995	
C-distance	0.1781	1	0.1781	0.2323	0.6402	
D-current density	50.22	1	50.22	65.49	< 0.0001	**Significant**
AB	2.18	1	2.18	2.84	0.1230	
AC	6.68	1	6.68	8.71	0.0145	**Significant**
AD	1.88	1	1.88	2.45	0.1488	
BC	1.80	1	1.80	2.34	0.1570	
BD	0.1552	1	0.1552	0.2024	0.6624	
CD	0.1122	1	0.1122	0.1463	0.7101	
A^2	2.85	1	2.85	3.72	0.0827	
B^2	0.0010	1	0.0010	0.0013	0.9722	
C^2	0.7063	1	0.7063	0.9211	0.3598	
D^2	1.16	1	1.16	1.51	0.2474	
Residual	7.67	10	0.7668			
Cor Total	92.07	24				

Table 8 Fit statistics for specific energy demand quadratic model.

R^2	Adjusted R^2	Predicted R^2	Adeq Precision
0.9167	0.8001	0.4751	9.9770

Specific Energy Demand=10.89 – 0.0983 *A +0.0002 *B –0.1273 *C + 2.23*D +0.7375 * AB –1.29 *AC –0.6850*AD –0.6700* BC –0.1970*BD – 0.2101 *CD+ 0.9300*A^2 –0.0173*B^2 –0.5059*C^2 – 0.6210* D^2 (5)

Powder Productivity Model

A model was created to optimize the efficiency of powder production. Table 9 presents the ANOVA results for the quadratic model of powder productivity. A model with an F-value of 4.46 is considered statistically significant. There is only a 1.12% chance that an F-value this large could occur due to noise. The significance values of "Prob > F′′ are less than 0.05, indicating that the model terms are considered significant. Based on these findings, it can be inferred that (C), (B^2), (C^2), and (D^2) are significant model terms. Table 10 shows the fit statistics for the powder productivity quadratic model. The Predicted R^2 of 0.0674 is not as close to the Adjusted R^2 of 0.6688 as one might normally expect. Adeq Precision measures signal-to-noise a ratio greater than 4 is desirable. In this mode, the ratio of 8.975 indicates an adequate signal. This model can be used to navigate the design space.

Table 9 ANOVA for productivity quadratic model.

Source	Sum of Squares	df	Mean Square	F-value	p-value	
Model	0.1007	14	0.0072	4.46	0.0012	**Significant**
A-temperature	0.0070	1	0.0070	4.32	0.0645	
B-rpm	0.0016	1	0.0016	0.9841	0.3446	
C-distance	0.0433	1	0.0433	26.83	0.0004	**Significant**
D-current density	0.0033	1	0.0033	2.02	0.1852	
AB	0.0003	1	0.0003	0.1688	0.6898	
AC	0.0047	1	0.0047	2.91	0.1189	
AD	0.0000	1	0.0000	0.0262	0.8746	
BC	1.000E-06	1	1.000E-06	0.0006	0.9806	
BD	0.0002	1	0.0002	0.1490	0.7076	
CD	0.0036	1	0.0036	2.22	0.1674	
A^2	0.0042	1	0.0042	2.63	0.1361	
B^2	0.0095	1	0.0095	5.90	0.0355	**Significant**
C^2	0.0085	1	0.0085	5.25	0.0449	**Significant**
D^2	0.0172	1	0.0172	10.67	0.0085	**Significant**
Residual	0.0161	10	0.0016			
Cor Total	0.1169	24				

Table 10 Fit statistics for powder productivity quadratic model.

R^2	Adjusted R^2	Predicted R^2	Adeq Precision
0.8620	0.6688	0.0674	8.9748

From the previous table, the final mathematical model for the powder productivity in terms of coded factors as indicated by design expert software is shown below:

Powder Productivity = 0.8879+ 0.0241*A+ 0.0115*B + 0.0627*C –0.0083*AB +0.0343*AC –0.0032*AD + 0.0005*BC + 0.0077*BD –0.0375*CD – 0.0359*A^2 – 0.0537*B^2 – 0.0554*C^2 – 0.0757*D^2 (6)

Actual and Predicted Values

Figure 3 presents the relationship between the actual and predicted values of cathodic current efficiency, specific energy demand, and powder productivity. This graph illustrates that the constructed models are adequate because the residuals in expectation for each response are minimized. This is evident as the residuals tend to cluster close to the diagonal line, indicating that the model accurately represents the response within the scope of the examined factors.

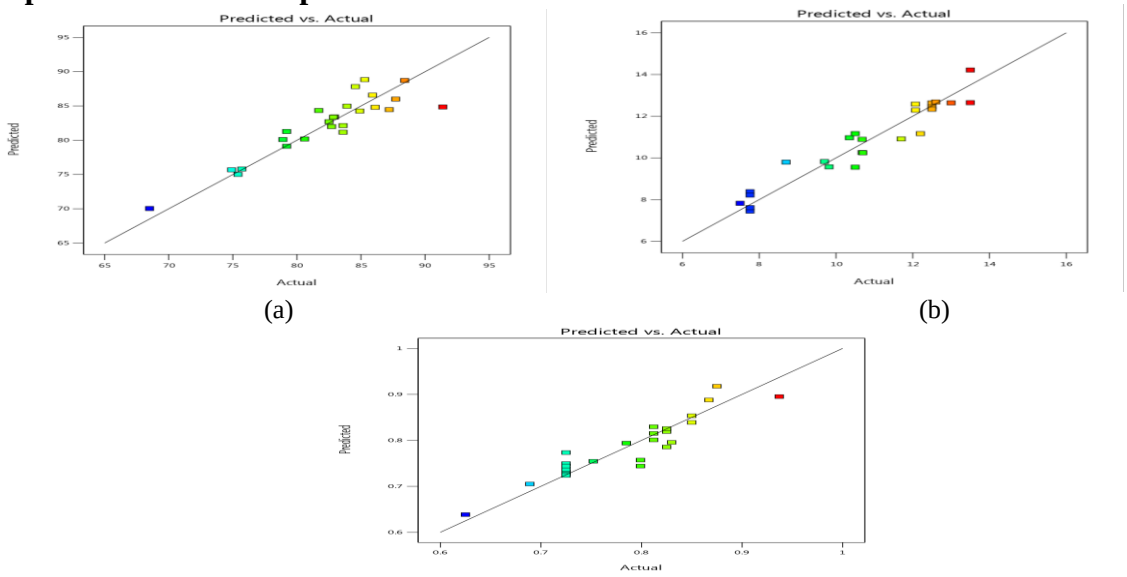

Fig. 3 Scatter diagrams of (a) cathodic current efficiency, (b) specific energy demand, and (c) powder productivity.

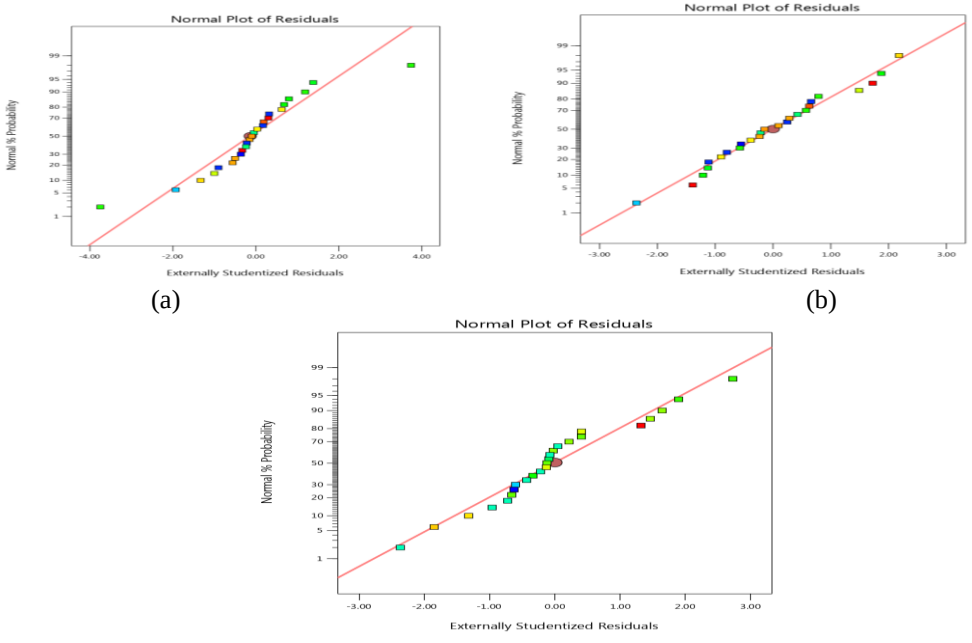

Fig. 4 Residual plots of the models of (a) cathodic current efficiency, (b) specific energy demand, and (c) powder productivity.

Figure 4 shows the normal plot of residuals of cathodic current efficiency, specific energy demand, and powder productivity. The majority of the points fall either directly on the straight line or very near to it, with only a few outliers. This demonstrates that the models are indeed efficient and accurate.

The perturbation plots illustrating how process parameters impact process responses can be found in Fig. 5. Perturbation plots highlight the effect of varying each parameter (temperature, stirring rate, distance, current density) on cathodic efficiency, energy demand, and productivity. For instance, current density and temperature show a significant impact on efficiency and energy demand. From Fig. 5, it was concluded that these plots demonstrate that current density and temperature are among the most influential parameters for optimizing electrowinning. This finding guides the focus on controlling these parameters precisely to achieve targeted efficiencies and productivity with minimal energy.

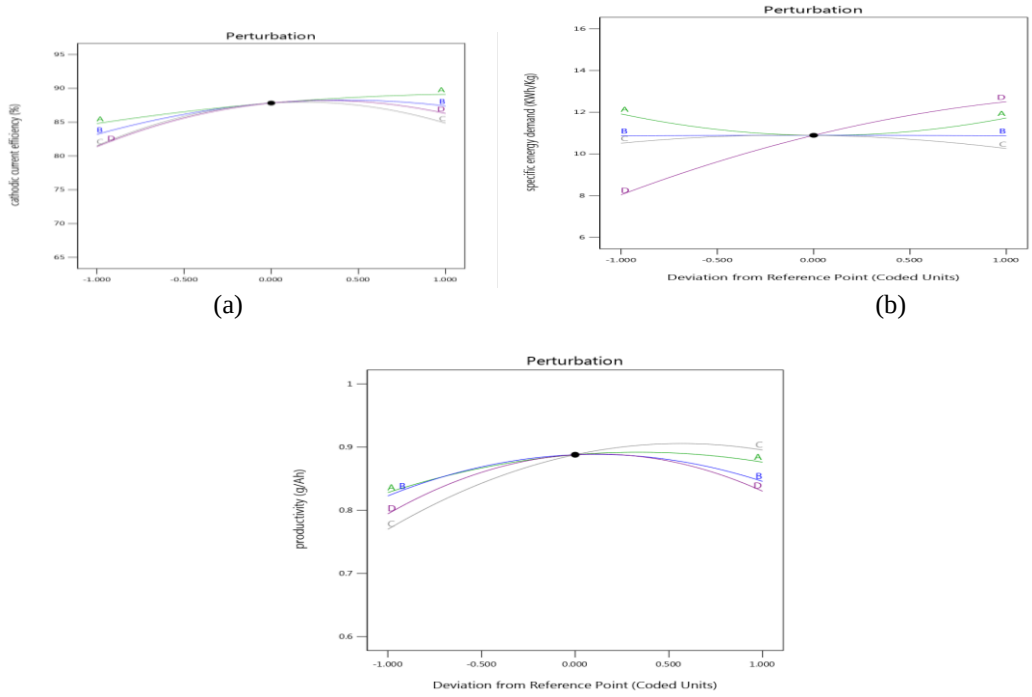

Fig. 5 Perturbation of the models of (a) cathodic current efficiency, (b) specific energy demand, and (c) powder productivity.

Effect of process parameters interactions on the process responses

One key difference between the statistical approach and experimental technique is the ability of the statistical approach to demonstrate how interactions between process parameters affect process responses. The contour and 3D surface plots are shown from Figs. 6 - 17. Contour plots visually represent the effect of different variables on a flat surface, while 3D surface plots take this representation a step further by adding shape to the color and contour information provided in the contour plot. Figs. 6 - 9 show the interactions between temperature and stirring rate, temperature and distance, and other parameters on responses like cathodic current efficiency, energy demand, and productivity. Higher temperatures and moderate

stirring rates are linked to improved efficiency and productivity. From these figures it was concluded that interaction plots suggest that the best results occur under specific parameter combinations. For instance, balancing higher temperatures with moderate stirring enhances process efficiency. This highlights the need to adjust parameters concurrently rather than in isolation to achieve desired outcomes.

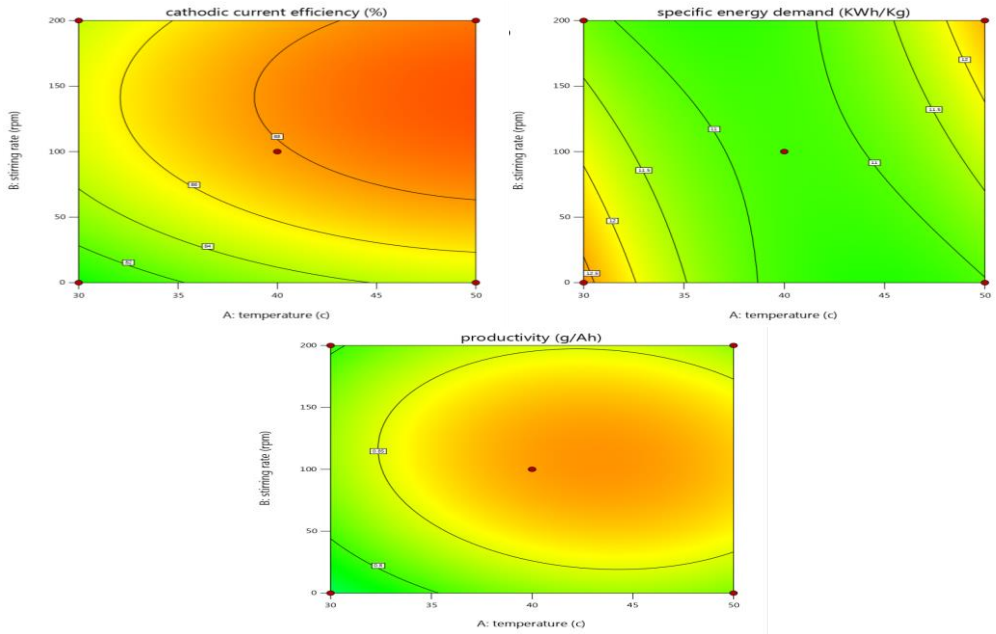

Fig. 6 Contour shows the effect of A and B on different responses.

In Fig. 7 the 3D surface plot illustrates the effect of temperature and stirring rate on cathodic current efficiency. The efficiency increases as the temperature and stirring rate rise, with the highest efficiency observed at higher temperatures and moderate stirring rates. This indicates that both parameters play a crucial role in optimizing the electrochemical process.

Also in this 3D surface plot, the interaction between temperature (A) and stirring rate (B) is shown and focuses on how they affect the specific energy demand (kWh/Kg). The plot suggests that specific energy demand varies with changes in both temperature and stirring rate. The contours at the base highlight that higher specific energy demand is observed at lower temperatures and higher stirring rates, as indicated by the color gradient shifting from green to yellow-red points on the surface likely representing key experimental data points or specific observation 3D surface plot, the interaction between temperature (A) and stirring rate (B) is explored plot shows that productivity (g/Ah) increases as the temperature and stirring rate change. The contour at the base of the plot reveals that the optimal combination of higher temperatures and moderate stirring rates leads to the highest productivity. The color gradient also suggests that productivity increases as the surface color shifts from green to yellow and orange. Points on the plot indicate actual data values, where those above or below the surface represent the difference between observed and predicted values.

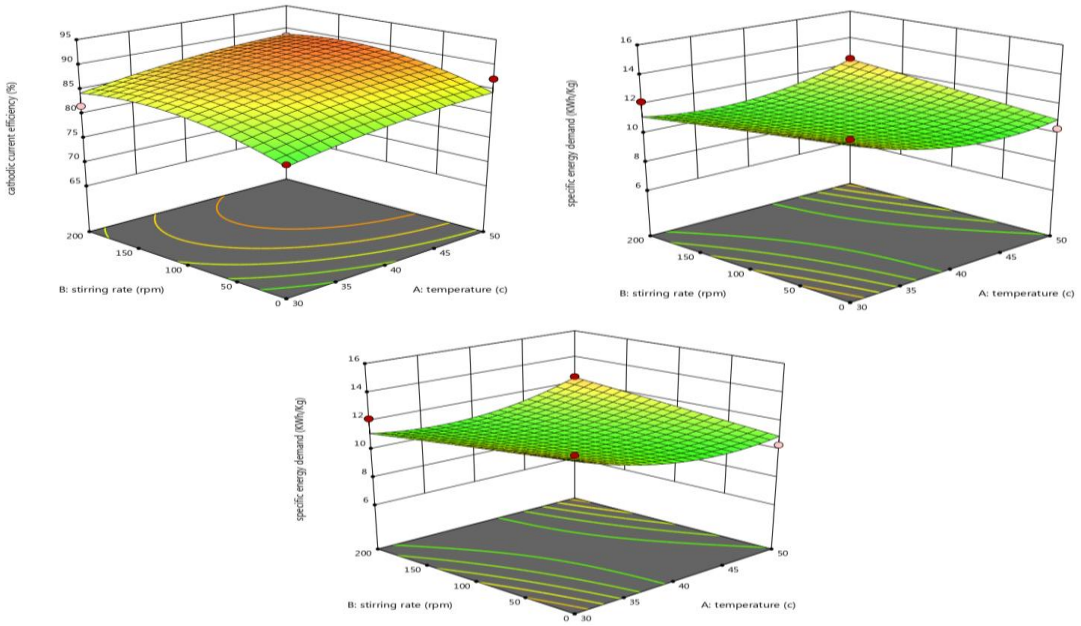

Fig. 7 D Surfacelots show the effect of A and B on different responses.

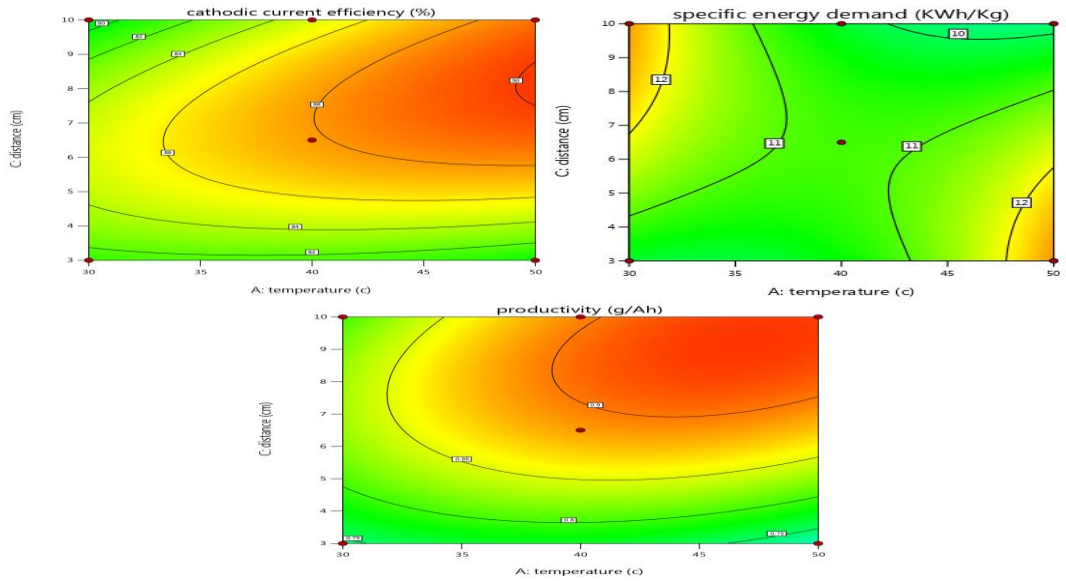

Fig. 8 Contour shows the effect of A and C on different responses.

In Fig. 9, The 3D surface plot shows how temperature and the distance between electrodes affect cathodic current efficiency. As the temperature rises, the efficiency improves, especially when the distance is set to a lower level, the results highlight that maintaining an appropriate distance, along with a controlled temperature, is essential for achieving higher efficiency levels in the process. This 3D surface plot illustrates the interaction between temperature (°C), distance (cm), and specific energy demand (KWh/kg). The graph shows that as the temperature increases, the specific energy demand decreases. Although the distance parameter has a less significant impact, it still has a measurable effect on energy demand. Key data points are highlighted to emphasize the trends across various conditions. This model helps in understanding

how these variables interact and provides insights into optimizing parameters for improved efficiency. Also, the 3D surface plot demonstrates the effect of temperature (A) and distance (C) on the productivity. The highest productivity values are observed at intermediate temperature and distance levels, as shown by the peak in the surface. The design points marked above and below the surface suggest that the experimental data align well with the model predictions, confirming that productivity increases as both parameters are optimized within a specific range. This 3D surface plot highlights the relationship between temperature (A) and distance (C) on productivity (g/Ah) under controlled conditions. The plot shows a curvature, indicating that increasing the temperature while keeping the distance at certain levels improves productivity. However, excessive changes in either parameter led to a decline in productivity, suggesting an optimal range for maximizing efficiency.

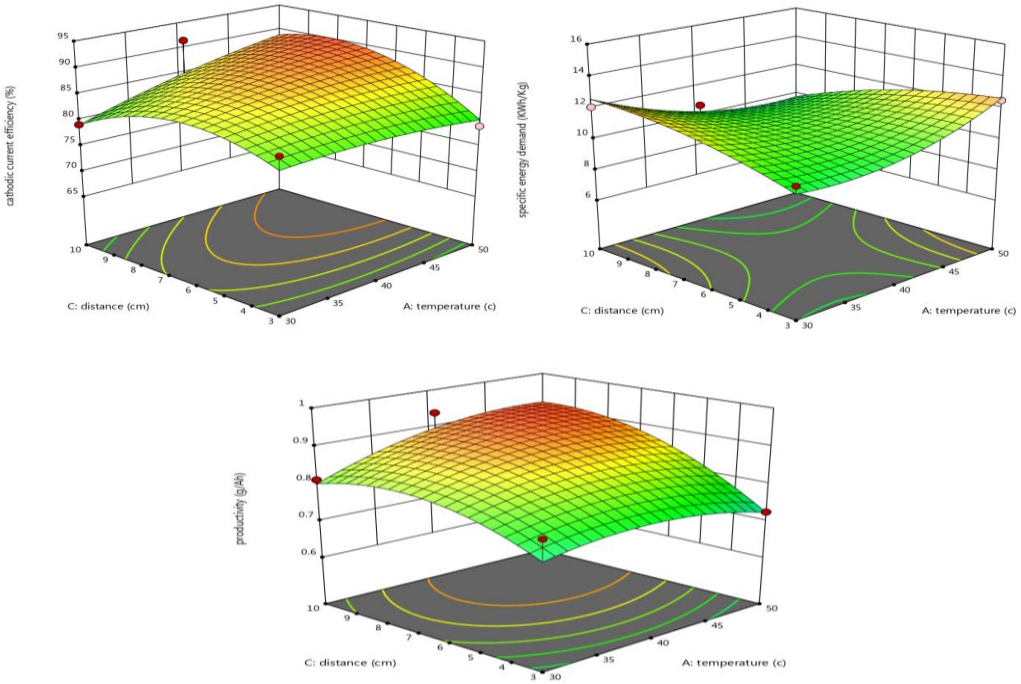

Fig. 9 3D surface plots show how effect of A and C on different responses.

Figures 10 - 15 illustrates additional parameter effects, such as current density with distance and stirring rate with current density. These plots reveal that lower distances and higher current densities significantly enhance efficiency, while specific stirring rate and current density combinations reduce energy demands. It was concluded that the contour plots reveal that certain parameter ranges lead to maximum efficiency and productivity. For example, decreasing the distance between electrodes while maintaining moderate stirring boosts the rate of manganese deposition. These insights provide specific guidelines for parameter tuning.

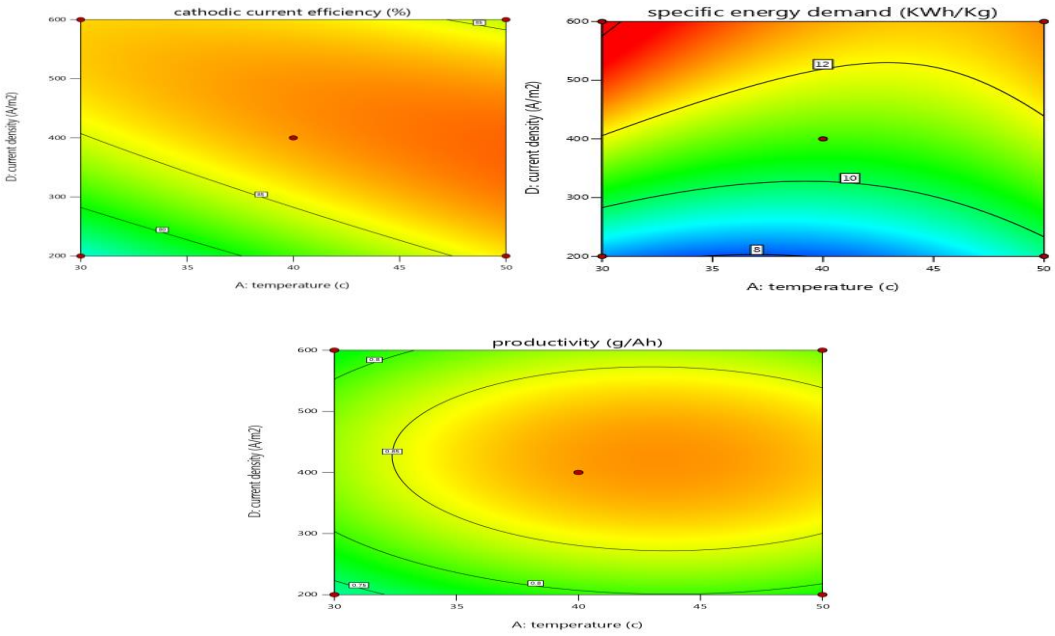

Fig. 10 Contourshows effect of A and D on different responses.

In Fig. 11, this plot highlights the relationship between temperature and current density in influencing cathodic current efficiency. As the temperature and current density increase, there is a noticeable rise in efficiency, reaching optimal values in specific ranges. This finding underscores the importance of balancing both temperature and current density to optimize the electrochemical process. This 3D surface plot shows the relationship between temperature (A: °C) and current density (D: A/m^2) on specific energy demand (kWh/kg). The plot suggests that as temperature increases, the specific energy demand tends to decrease, indicating that higher temperatures lead to lower energy consumption. In contrast, as current density increases, the specific energy demand generally rises, meaning higher current densities require more energy. The interaction between these two variables is visually represented by the color gradient, with blue indicating lower specific energy demand and red representing higher values. This visualization helps in identifying the optimal temperature and current density combination for minimizing energy use. In this 3D surface plot, the interaction between temperature (A) and current density (D) is examined. The plot suggests that productivity (g/Ah) increases with higher temperature and lower current density. The elliptical contour at the base of the plot shows this relationship, where the optimal combination of higher temperature and moderate current density results in the highest productivity levels.

Fig. 13 shows a 3D surface plot that visualizes the interaction between stirring rate (B) and distance (C) on cathodic current efficiency. The efficiency increases with lower stirring rates and greater distances between electrodes, achieving a peak efficiency above 85%. This 3D surface plot shows the relationship between stirring rate (B: rpm) and distance (C: cm) on specific energy demand (kWh/kg). The plot reveals that as the stirring rate increases, the specific energy demand tends to rise,

indicating that higher stirring rates require more energy. On the other hand, the effect of distance on specific energy demand is less pronounced, but it still influences the energy demand, with certain distances leading to lower or higher energy consumption depending on the stirring rate. The contour lines and color gradient on the plot help visualize these interactions, showing how varying combinations of stirring rate and distance impact energy and efficiency.

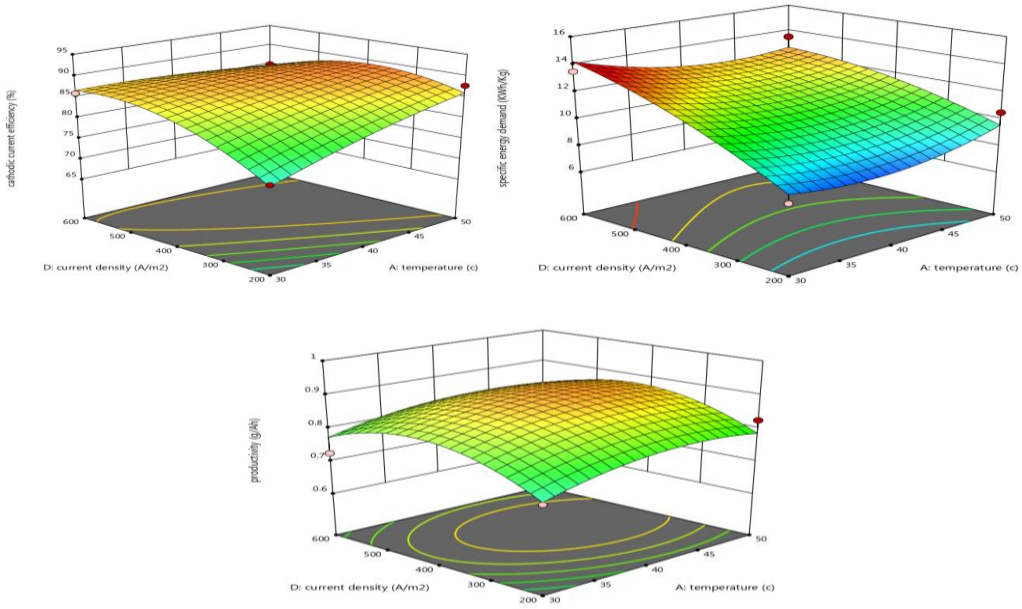

Fig. 11 3D surface plots the show effect of A and D on different responses.

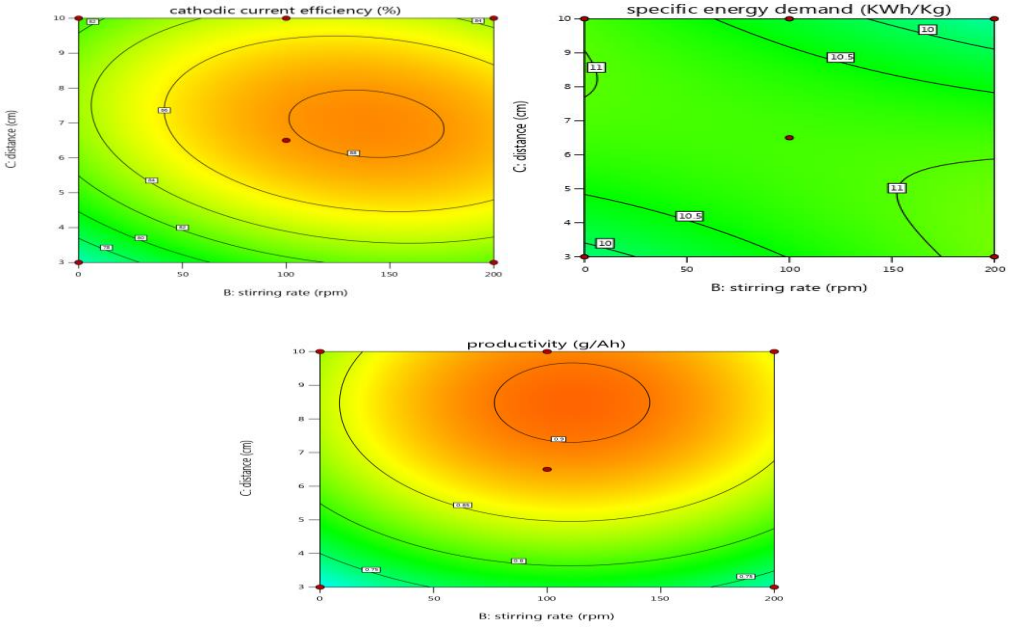

Fig. 12 Contour shows the effect of B and C on different responses.

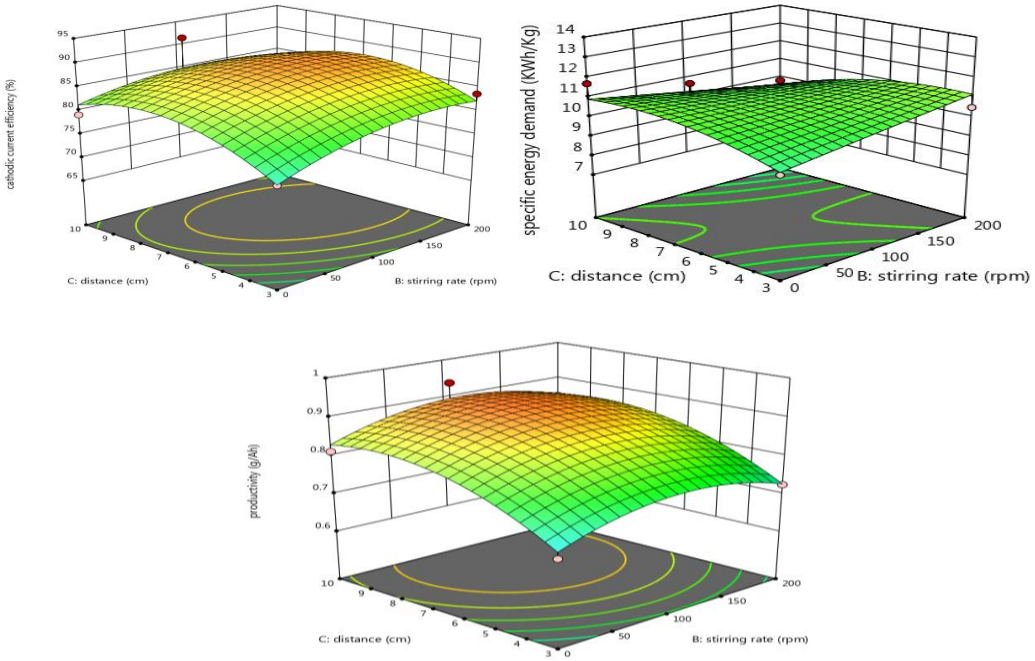

Fig. 13 3D surface plot shows the effect of B and C on different responses.

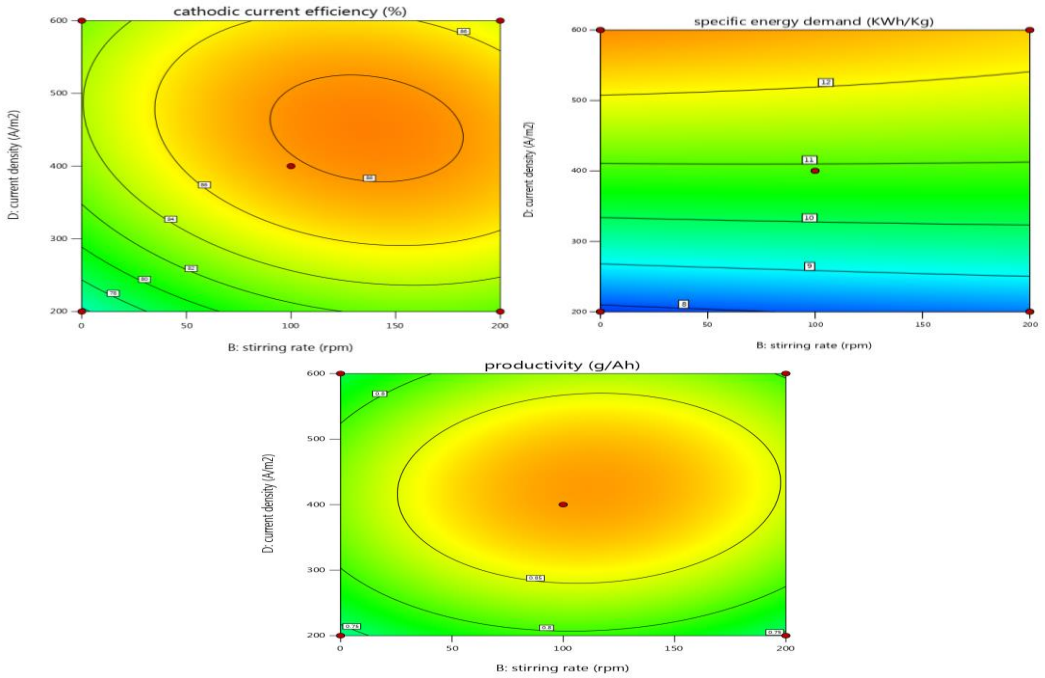

Fig. 14 Contour shows the effect of B and D on different responses.

The 3D surface plot shown in Fig. 15 illustrates the relationship between stirring rate (B) and current density (D) on cathodic current efficiency. Higher current density and lower stirring rates lead to an increase in efficiency, with a maximum close to 90 %.

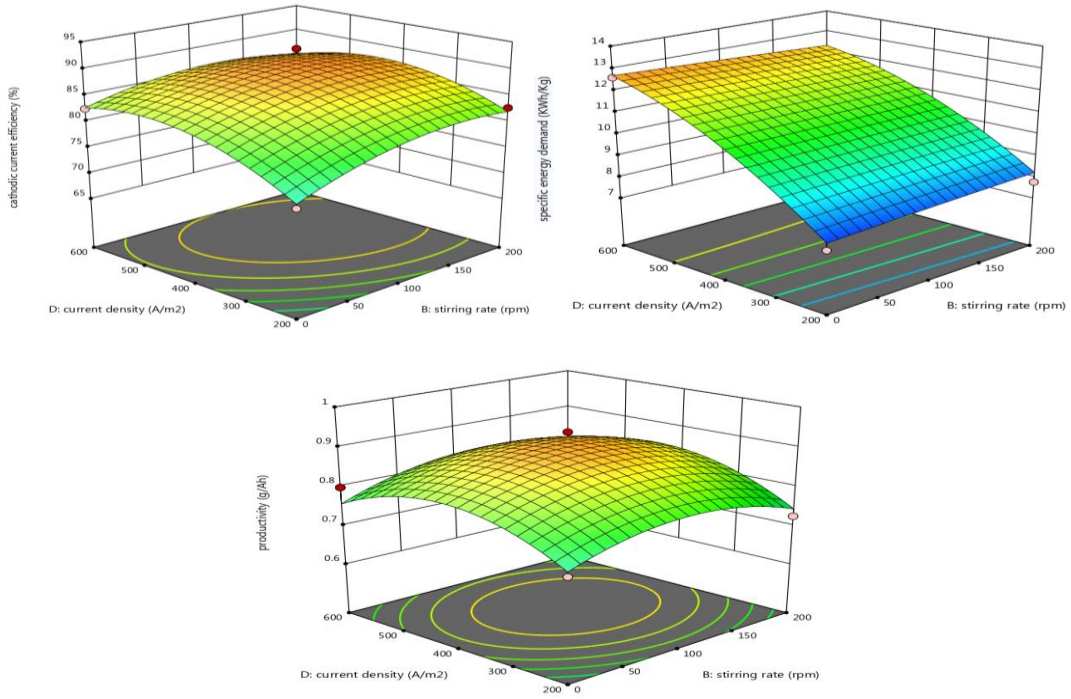

Fig. 15 3D surface plots the show effect of B and D on different responses.

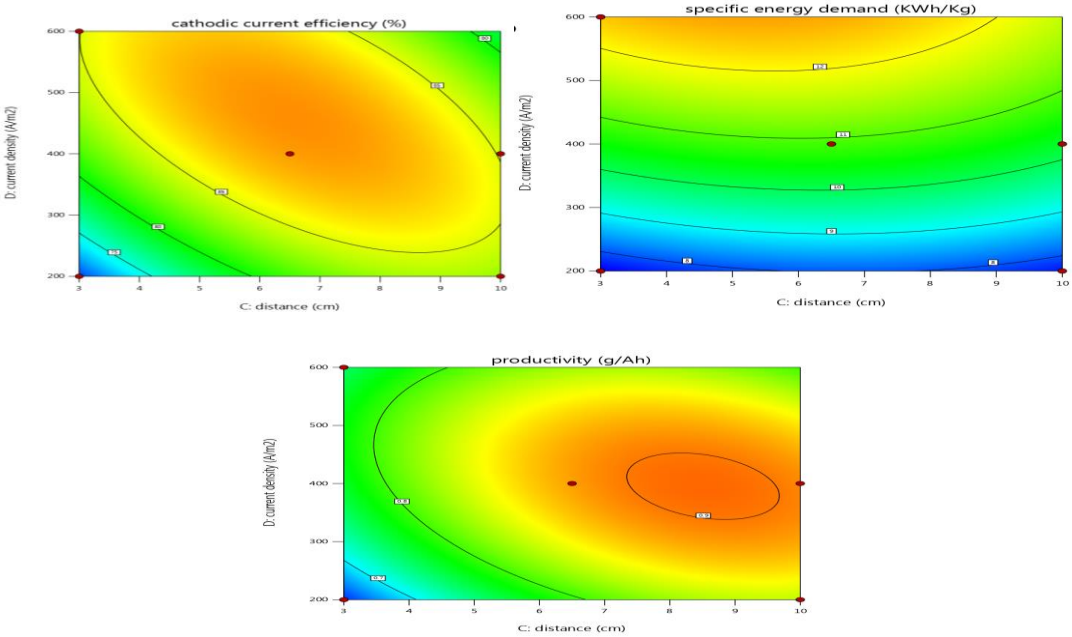

Fig. 16 Contour shows the effect of C and D on different responses.

This 3D surface plot shows the variation in cathodic current efficiency (%) as a function of distance (C) and current density (D). The graph suggests that higher current density and a smaller distance between electrodes result in higher efficiency, peaking at around 90 %. The design points show values that are both above and below

the surface, indicating the spread of data used for the optimization process as shown in Fig. 17.

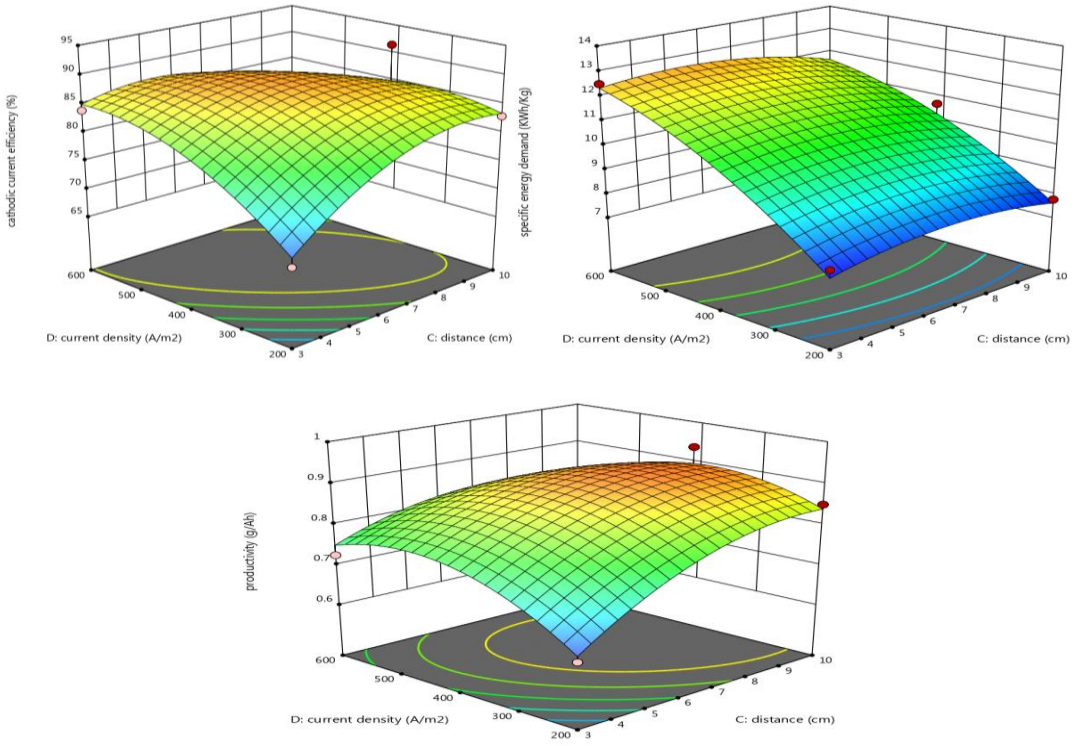

Fig. 17 3D surface plots show the effect of C and D on different responses.

The previous figures show how temperature, stirring rate, and process responses are related. It is observed that increasing both the temperature to 40 and 50 ℃ and the stirring rate up to 100 rpm can enhance the cathodic current efficiency. Also increasing the distance between the anode and the cathode can enhance the cathodic current efficiency and powder productivity. According to Fig.10 and Fig.11, the highest cathodic current efficiency occurs at a high current density, but significantly decreases at lower current densities and temperatures as happened in an optimization of packed bed electrolysis of zinc anode casing of spent dry cell batteries.

Optimization of the Packed Bed Electrolysis Process

In this research, the optimization methods used involved merging the objectives into a single desirability function to predict the desired outcomes for each factor and response through numerical and graphical techniques. The goals of optimization can be utilized to maximize, minimize, or achieve the desired value of the response variable, [33].

Single Response Optimization

The established models were utilized to optimize the input parameters of the packed bed electrolysis process. Each model was independently optimized without considering the other responses. Table 11 shows the single response optimization criteria for input/output process parameters. This table displays the relative significance of each factor that has been chosen.

Table 11 Single response optimization criteria for input/output process parameters.

Criteria	Parameters				Responses		
	A,℃	B, rpm	C, cm	D, A /m^2	CE,%	SE, Wh/Kg	PP,g/Ah
1	Min (+++)	Min (+++)	Min (+++)	Min (+++)	Max (+++)	_	_
2	Min (+++)	Min (+++)	Min (+++)	Min (+++)	_	Max (+++)	_
3	Min (+++)	Min (+++)	Min (+++)	Min (+++)	_	Min (+++)	_
4	Min (+++)	Min (+++)	Min (+++)	Min (+++)	_	_	Max(+++)
5	Min (+++)	Min (+++)	Min (+++)	Min (+++)	Min (+++)	_	_
6	Min (+++)	Min (+++)	Min (+++)	Min (+++)	_	_	Min (+++)

Numerical Optimization

In this study, four optimization criteria were selected. A multi-criteria optimization approach was utilized to optimize the input and output process parameters for each criterion.

Graphical Optimization

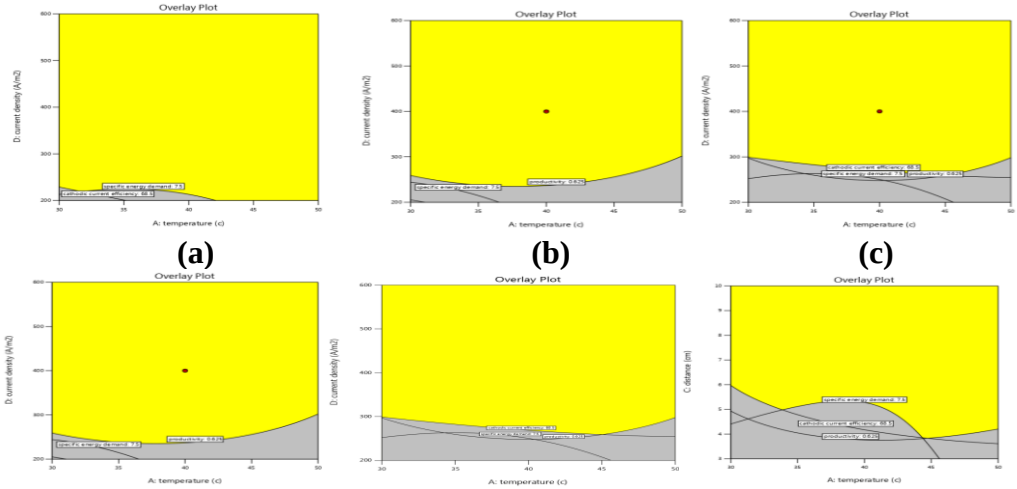

(a) (b) (c)

(d) (e) (f)

Fig. 18 Overlay plots show the region of the optimal process conditions of:

(a) criteria (1)
(b) criteria (2)
(c) criteria (3)
(d) criteria (4)
(e) criteria (5)
(f) criteria (6)

Graphical optimization with multiple responses identifies specific areas where requirements meet the proposed criteria simultaneously. By overlaying critical response contours on a plot, it becomes feasible to visually search for the optimal compromise. Therefore, when dealing with multiple responses, it is advisable to conduct numerical optimization first. The graphical optimization showcases the achievable response values within the factor space. The overlay plots in Fig. 18 demonstrate how graphical optimization enables the visual selection of the best process conditions based on specific criteria. The results of the graphical optimization are shown in overlay plots, which are very convenient for quickly choosing the

parameter values for the packed bed electrolysis process to achieve desired response values. The shaded yellow areas on the overlay plot in Fig. 18 indicate the regions that satisfy the specified criteria.

The results of the graphical optimization are shown in overlay plots, which are very convenient for quickly choosing the parameter values for the packed bed electrolysis process to achieve desired response values. The shaded yellow areas on the overlay plot in Figure 18 indicate the regions that satisfy the specified criteria. The overlay plot visually pinpoints the specific parameter combinations where all criteria converge, indicating the most balanced operating conditions. This region offers practical ranges for multi-criteria optimization, ensuring efficient resource use and effective manganese recovery.

2 Desirability

The desirability function method is widely used in modern industrial applications to optimize multiple response processes by identifying the optimal working conditions that yield the most desirable outcomes. The primary objective of the optimization method is to find a set of conditions that satisfy all goals, rather than just achieving a desirability value of 1.0, [25]. Table 12 shows the optimization criteria and optimization results using numerical multiple responses. The desirability values and graphs of the six optimization criteria are shown in Fig.19. These desirability values confirm the model's strength in predicting conditions that optimize the electrowinning process across multiple responses. Achieving high desirability indicates that the identified parameter ranges effectively satisfy all process objectives, including efficiency, productivity, and minimal energy use.

Table 12 The optimization criteria and optimization results using numerical multiple responses.

Criteria	Parameters				Response			Desirability
	A	B	C	D	CE	SE	PP	
1	30	29.511	4.062	389.651	79.474	10.877	0.738	0.712
2	30	0	4.627	380.120	77.843	11.186	0.72	0.763
3	30	0.002	3	200.156	59.670	6.357	0.545	1
4	31.862	36.403	5.056	315.225	78.220	9.935	0.761	0.695
5	30	0.043	3.004	200.001	59.675	6.357	0.545	1
6	30.016	0.974	3	200.001	59.751	6.353	0.546	0.999

3 Validation of the Experiments

Tables 13, 14, and 15 were carried out to evaluate the reliability of the statistical work. As shown in Tables 13,14, and 15, all values are in the range of engineering errors and accepted in the industry. Also, Fig.20, Fig.21, and Fig.22 show these values. The percentages of error can be calculated from the following equation :

$$\text{Error},[E] = \frac{Actual\ Value - Predict\ Value}{Actual\ Value} \quad \text{x100} \qquad (7)$$

From Figs. 20 - 22 it was shown that the low error rates validate the model's predictive accuracy for key performance metrics. This reliability in prediction underscores the model's potential for application in real-world settings, where achieving consistent results is critical for scaling the electrowinning process.

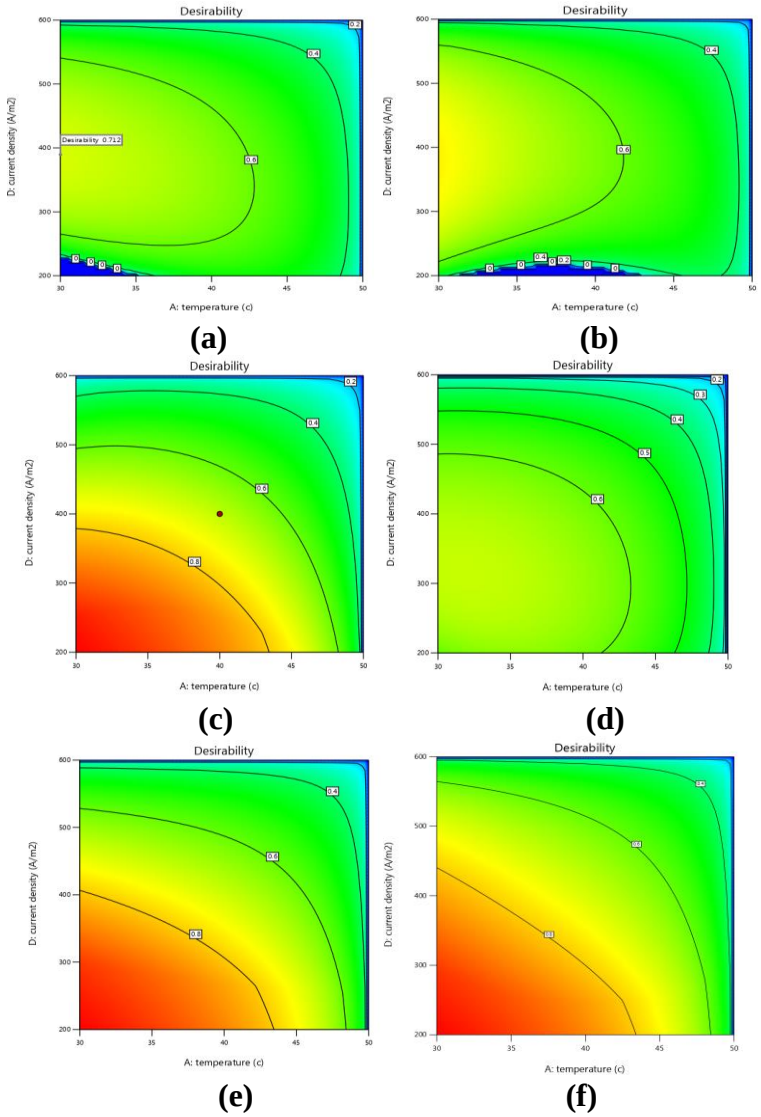

Fig. 19 Desirability graphs of the models, (a) criteria (1), (b) criteria (2), (c) criteria (3), (d) criteria (4), (e) criteria (5) and (f) criteria (6).

Table 13 Validation for the cathodic current efficiency response.

Run	A, °C	B, Rpm	C, cm	D, A/m^2	Actual Value	Predict Value	Error [E]%
6	30	100	10	400	79.2	79.12	0.1
8	40	100	10	200	82.93	83.4	0.5
9	40	100	6.5	400	84.56	87.83	3.8
15	40	200	10	400	82.85	83.36	0.6
16	40	0	10	400	79.2	81.27	2.6
18	50	100	10	400	85.85	88.85	3.4
24	40	100	10	400	91.38	84.85	7.1

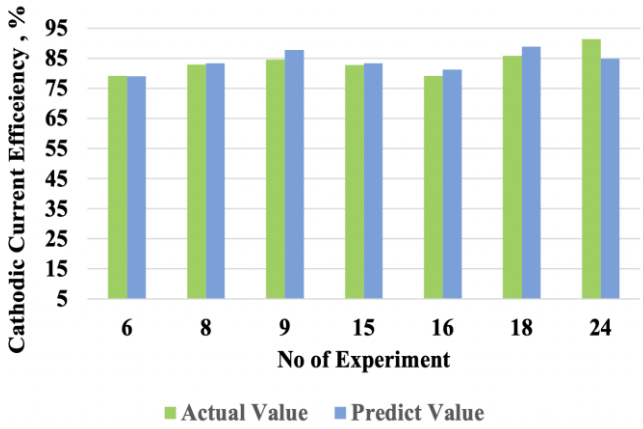

Fig. 20 Validation for the cathodic current efficiency response.

Table 14 Validation for the specific energy demand response.

Run	A, ° C	B, Rpm	C, Cm	D, A/m^2	Actual Value	Predict Value	Error [E]%
6	30	100	10	400	12.07	12.58	4.2
8	40	100	10	200	7.76	7.61	1.9
9	40	100	6.5	400	10.68	10.89	1.9
15	40	200	10	400	9.82	9.57	2.5
16	40	0	10	400	11.70	10.91	6.7
18	50	100	10	400	8.70	9.80	12.6
24	40	100	10	400	10.68	10.26	3.9

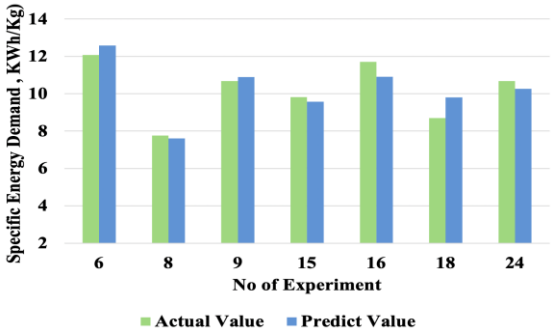

Fig. 21 Validation for the cathodic current efficiency response.

Table 15 Validation for the productivity response.

Run	A, ° C	B, rpm	C, cm	D, A/m^2	Actual Value	Predict Value	Error [E]%
6	30	100	10	400	0.812	0.8010	1.35
8	40	100	10	200	0.85	0.8390	1.29
9	40	100	6.5	400	0.8670	0.8879	2.41
15	40	200	10	400	0.85	0.8535	0.411
16	40	0	10	400	0.812	0.8295	2.155
18	50	100	10	400	0.875	0.9177	4.88
24	40	100	10	400	0.937	0.8952	4.46

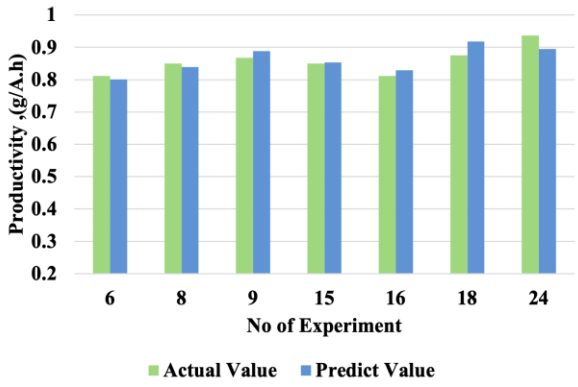

Fig. 22 Validation for the productivity response.

CONCLUSIONS

1. Statistical modeling and optimization of the electrowinning process were carried out to recycle spent $ZnMnO_2$ batteries, to produce high-quality electrolytic zinc powders. The investigation yields the following conclusions:

2. The suggested models effectively forecast responses within the specified parameters of the process being applied.

3. The current density, stirring rate, temperature, the distance between the anode and the cathode, and the two-level interactions of temperature and current density are the most significant model terms associated with cathodic current efficiency.

4. The optimum conditions of the electrowinning process are temperature electrolyte =40℃, stirring rate=100 rpm, the distance between the anode and the cathode= 10 cm, and current density =400 A/m^2.

5. RSM can be considered a powerful tool in the optimization of the electrolysis of paste of the $ZnMnO_2$ of spent primary batteries.

REFERENCES

1. **Dell R. M., ‘’Batteries: fifty years of materials development." Solid State Ionics, vol. 134, pp. 139-158, (2000).**
2. **Zhao S., An H., Chen S., "A study of a high-power ammonium chloride zinc /manganese dioxide dry battery." Journal of Power Sources, vol. 76, pp. 218-220, (1998).**
3. **Bernardes A.M., Espinosa D.C.R., Tenorio J.A.S., "Recycling of batteries: a review of current processes and technologies." Journal of Power Source, vol. 130 , pp. 291-298, (2004).**
4. **Wei Z., Cheng J., Wang R., Li Y., Ren Y., "From spent Zn-MnO_2 primary batteries to rechargeable Zn-MnO_2 batteries: a novel directly recycling route with high battery performance." Journal of Environmental Management, vol.298, pp. 113473, (2021).**
5. **"user: l head holder Wikimedia common simplified diagram of alkaline battery construction." 2021. https://commons.wikimedia.org/wiki/file:alkaline-battery-english.svg (accesseMarchch 19, (2020).**

6. **Espinosa D.C.R., Bernardes A.M., Tenrio J.A.S., "An overview on the current processes for the recycling of batteries." Journal of Power Sources, vol. 13, pp. 311-319, (2004).**
7. **Sayilgan E., Kukrer T., Civelekoglu G., Ferella F., Akcil A., Veglio F., Kitis M., "a review of technologies for the recovery of metals from spent alkaline and zinc -carbon batteries." Hydrometallurgy, vol. 97, pp. 158-166, (2009).**
8. **Murugappan R.M., Karthikeyan M., "Microble assisted management and recovery of heavy metals from electronic wastes." environmental management of waste electronic equipment, pp. 65-88, (2021).**
9. **Owais A., "Electrowinning of lead powder from chloride leach liquor." world of Metallurgy vol. 65 , pp. 361-367, (2012).**
10. **Owais A., Bernd F.,"packed bed electrolysis for production of copper powder." world of metallurgy, vol. 6, pp.668-677, (2003).**
11. **Owais A., "effect of material and shape of starting cathodes on electrowinning of copper powder." JPME, pp. 13-21, (2007).**
12. **Owais A., "production of electrolytic copper powder from brass scraps." JPME, pp. 35-43, (2007).**
13. **Owais A., "effect of electrolyte characteristics on electrowinning of copper powder." J. Appl Electrochem, vol 39, pp. 1587-1595, (2009).**
14. **Owais A., Mohamed A.H.G, Ahmed E., "production of electrolytic zinc powder from zinc anode casing of spent dry cell batteries." Hydrometallurgy, vol. 157, pp. 60-71, (2015).**
15. **Roriz E.R.R., Espinosa D.C.R., Tenorio J.A.S., "Battery recycling: effect of current density on manganese recovery through an electrolytic Brazilian Journal of chemical engineering, vol. 3, pp.271-277, (2016).**
16. **Makhanbetov A., Zharmenov A., Bayeshov A., Mishra B., Baigenzhenov O., "production of electrolytic manganese from sulfate solutions." metallurgy of nonferrous metals, vol. 5, pp. 606-610, (2015).**
17. **Owais A., Ahmed E., Dardeir A., Gepreel M.A.H., "production of electrolytic manganese powder from Egyptian low-grade manganese ore." world of Metallurgy, vol. 5,pp. 285-292, (2019).**
18. **Sahoo R., Naik P., Das S., "Leaching of manganese from low-grade manganese ore using oxalic acid as a reductant in sulphuric acid solution." Hydrometallurgy, vol.62, pp. 157-163 ,(2001).**
19. **El Hazek M. N., Lasheen T.A., Helal A.S., "Reductive leaching of manganese from low-grade Sinai ore in HCL using H_2O_2 as reductant." Hydrometallurgy, vol .4, pp. 187-191, (2006).**
20. **Zhang Y., You Z., Li G., Jiang T.,"Manganese extraction by sulfur-based reduction roasting acid leaching from low-grade manganese oxide ores." Hydrometallurgy, vol. 13, pp. 126-132, (2013).**
21. **Somasundaram M., Saravanathamizhan R., Basha C.A., Nandakumar V., Begum S.N., Kannadasan T.,''recovery of copper from scrap printed circuit board: modeling and optimization using response surface methodology.'' Powder Technol, vol. 266, pp. 1–6, (2014).**

22. **Virkutyte J., Rokhina E., Jegatheesan V.,''Optimisation of electro -fenton denitrification of a model wastwater using a response surface methodology'' Bioresour. Technol, vol. 101,pp. 1440–1446, (2010).**
23. **Li M., Feng C., Zhan Z., Che R., Gao C., Sugiura N., ''Optimization of process parameters for electrochemical nitrate removal using Box-Behnken design.'' Electrochim Acta, vol.56,pp. 265–270, (2010).**
24. **Li M., Feng C., Zhang Z., Liu X., Ma W., Xue Q., Sugiura N., ''optimization of electrochemical ammonia removal using Box-Behnken design''. J. Electroanal Chem, vol. 657, pp. 66–73, (2011).**
25. **Uwe R., Marku S., Oleg M., Ahmed E., "Optimization of laser welding of DP/TRIP steel sheets using statistical approach." Optics & Laser Technology, vol.44, pp. 255-262, (2012).**
26. **Said E.A.M., Abdel Ghafar H.M., Elsoeudy R.I., Ali S.A.M., Ahmed E., Owais A., "Purification of Mn-Electrolyte Solution from Leaching of Zn-MnO2 Spent Batteries Using Cementation Technique." Suez Canal Engineering Energy and Environmental Science Journal, vol.2, pp. 51-62, (2024).**
27. **Said E.A.M., Elsoeudy R.I., Ali S.A.M., Ahmed E., Owais A.,'' Production of Electrolytic Manganese Powder from Paste of $ZnMnO_2$ Spent Primary Batteries using Electrowinning Technique ''. (Under Publication)**
28. **Hao S., Zhang Ke., Zhengyi X., Huang T., Fan L., Weining B., ''Applying statistical models optimize the process of multi-pass narrow-gap laser welding with filler wire''. Int. J. Adv. Manuf. Technol, vol. 75 , pp.279–291, (2014).**
29. **Box G E P., Wilson K.B.J.R.''On the experimental attainment optimum conditions''. J. Royal Stat. Soc. B, vol. 13,pp.1–45, (1951).**
30. **Montgomery D.C., ''Design and analysis of ExperimentsEighthth ed''. Wiley, New York. , (2014).**
31. **Ahmed E., Owais A., "optimization of packed bed electrolysis of zinc anode casing of spent dry cell batteries. "Hydrometallurgy, vol.16 , pp. 176-191,(2016).**
32. **Gupta, Chiranjib K., "Chemical Metallurgy: p rinciples and practice, acquaintance." Wiely Vch (Wiely Vch), (2003).**
33. **Pasandideh S.H.R.P., Niaki S.T.A., ''Multi-response simulation optimization using genetic algorithm within desirability function framework." Appl Math Comput, vol .1, pp. 366-382, (2006).**